Atmospheric modeling study on convection-triggered teleconnections driving the summer North American dipole

Husile Bai,[a] Courtenay Strong,[a]

[a] *Department of Atmospheric Sciences, University of Utah, Salt Lake City, Utah*

Corresponding author: Courtenay Strong, Court.strong@utah.edu

Early Online Release: This preliminary version has been accepted for publication in *Journal of Climate*, may be fully cited, and has been assigned DOI 10.1175/JCLI-D-23-0015.1. The final typeset copyedited article will replace the EOR at the above DOI when it is published.

ABSTRACT: The summer North American Dipole (NAD) is a pattern of climate variability linked to variations in Boreal Forest seed production and migration of seed-eating birds. This is a modeling investigation of two teleconnections identified as drivers of the NAD in prior observational work: tropically-sourced atmospheric Rossby waves associated with anomalies in the phase distribution of the Madden Julian Oscillation (MJO) (i.e., phases 1 and 6 are anomalously prominent), and 2) a pan-Pacific atmospheric Rossby wave linked to east Asian monsoonal (EAM) convection. Sea surface temperature (SST) boundary forcing experiments were conducted with the Community Earth System Model 2 (CESM2) to trigger convection patterns which align with those observed during EAM and non-uniform phase distributions of MJO. For the EAM case, an El Niño–like SST dipole pattern combined with cool southern Japan SST forcing produced a convection and jet stream shift anomaly over East Asia and the northern Pacific with a positive NAD pattern downstream over North America, similar to the observed pattern when precipitation over East Asia (P_{EA}) is relatively high. A companion experiment with only ENSO-like SST forcing also produced the NAD but featured a different structure over the Eurasian continent with a response resembling the Summer East Atlantic (SEA) pattern over eastern North America and the eastern Atlantic. Simulation results suggest that the southern Japan SST forcing region has a secondary importance in triggering the NAD, producing only a somewhat NAD-like pattern by itself and only slightly improving the NAD produced by ENSO-like forcing. Simulations using SST forcing to induce seasonal convection anomalies with spatial patterns similar to anomalously frequent occurrence of MJO phase 1 (phase 6) produced circulation response patterns resembling the positive NAD (negative NAD).

Accepted for publication in *Journal of Climate*. DOI 10.1175/JCLI-D-23-0015.1.

1. Introduction

The tendency for climate variability to produce continental-scale juxtaposed positive and negative anomalies of temperature and precipitation is of increasing interest to ecological researchers focusing on phenology, reproduction, and migration (Zuckerberg et al. 2020). A specific example is the summer North American dipole (NAD) which entrains boreal bird irruptions (large, periodic movements of individuals outside their normal range) through climate-associated effects on conifer seed production (Strong et al. 2015; Bai et al. 2023). Such ecologically relevant dipoles can be teleconnected to larger scale modes of atmospheric variability such as the Pacific-North American pattern (PNA; Wallace and Gutzler 1981), Pacific-East Asian teleconnection (Wang et al. 2000), and circumglobal teleconenction (CGT) (Branstator 2002). Studying teleconnection mechanisms is thus important for understanding the origin of the climate dipoles that drive ecological and evolutionary processes and how they may evolve under projected climate change.

Although midlatitude teleconnections exhibit substantial internal variability, they are responsive to low latitude sea surface temperature (SST) anomalies, with PNA sensitivity to tropical Pacific SSTs being an example. There has been considerable effort devoted to understanding these atmosphere-ocean interactions over the global oceans (Alexander et al. 2002, 2004; Cassou et al. 2004). Heating and cooling anomalies of the surface oceans, such as those associated with the El Niño-Southern Oscillation (ENSO), significantly impact the atmospheric circulation in the tropics and extratropics as shown in observational (Namias 1976; Horel and Wallace 1981) and modeling (Palmer and Zhaobo 1985) studies. The geopotential height response to extratropical SST anomalies, by contrast, tends to be weaker and its sign depends on the involvement of eddies (Thomson and Vallis 2018). The Pacific-Japan (PJ) pattern is a specific example involving a meridional dipole of circulation and convective activities between the subtropical western Pacific near 20°N and the Japan Islands during the summer. Prior work on the PJ pattern has linked zonally elongated circulation anomalies over the Northern Pacific with enhanced precipitation over South of Japan (Nitta 1987; Kosaka and Nakamura 2010). It has also been reported that the tropical convective activity over the Indian Ocean and South China sea area in June and July has significant impact on the Pacific-Japan pattern (Kosaka and Nakamura 2006).

The Madden-Julian Oscillation (MJO) is one of the dominant sources of seasonal climate variability (Matthews 2004; Zhang 2005). During MJO events, deep convection migrates from the

Accepted for publication in *Journal of Climate*. DOI 10.1175/JCLI-D-23-0015.1.

Indian Ocean to the western Pacific region, resulting in consistently enhanced or suppressed convective systems over the equatorial belt (Matthews et al. 2004), and this pattern accounts for almost 50% of the tropical outgoing longwave radiation (OLR) variance (Kessler 2001). The MJO occurs in the tropics but has widespread impacts that affect climate over the subtropics and the midlatitudes through teleconnections. For example, the MJO has been found to influence seasonal convective anomalies in Australia (Wheeler et al. 2009), temperature and precipitation anomalies in the continental U.S. (Zhou et al. 2012), and dipole-like Rossby wave anomalies over North America (Tseng et al. 2019; Zhang 2013).

Despite extensive research on the connection between SST anomalies and climate anomalies, the dynamics and teleconnections associated with the ecologically-relevant North American Dipole (NAD) have not been studied in depth. Bai et al. (2023) investigated two mechanisms for the NAD based on observations. The first was a pan-Pacific Rossby wave triggered by east Asian monsoon (EAM) convection. The second mechanism relates to non-uniformity in the distribution of daily MJO phases during a given summer (most evident when inputs to the MJO algorithm are not low-pass filtered). The leading principal component of unfiltered MJO phases captured the tendency for phases 1 or 6 to be anomalously frequent, producing convection patterns which appeared to trigger positive and negative NAD, respectively. Modeling experiments are needed to test these hypothesized causal mechanisms, motivating the present study. Data and methods are presented in Section 2. The relationship between subtropical convection and North American climate dipole is shown in Section 3. The linkage between tropical oceanic forcing and NAD is presented in Section 4. Conclusions and discussions follow in Section 5.

2. Data and methods

a. Climate data

Reanalysis data sets from 1950 to 2019 for monthly average geopotential height were based on the National Centers for Environmental Prediction/National Centre of Atmospheric Research (NCEP/NCAR) Reanalysis (Kalnay et al. 1996), and the extended full century daily data for historical observational MJO analysis was obtained from NOAA PSL's 20th Century Reanalysis (NOAA-20CR) (Compo et al. 2006). The monthly mean Outgoing Longwave Radiation (OLR) data were from National Oceanic and Atmospheric Administration (NOAA) Physical Sciences

Accepted for publication in *Journal of Climate*. DOI 10.1175/JCLI-D-23-0015.1.

Laboratory (PSL) (Liebmann and Smith 1996), and sea surface temperatures (SSTs) were obtained from the Hadley Centre Sea Ice and Sea Surface Temperature dataset (HadISST) (Titchner and Rayner 2014).

b. Unfiltered Multivariate Madden-Julian oscillation (UMM)

We used the unfiltered-multivariate MJO indices (UMM1 and UMM2) defined by Bai et al. (2023). Briefly, it is calculated in a similar manner with Real-time Multivariate MJO (RMM) (Wheeler and Hendon 2004). We computed the EOF of combined daily OLR and the upper and lower layer zonal wind with removing the annual cycle and ENSO prior to the EOF analysis. But to understand how interannual-to-decadal variability in tropical convection influences the circulation response, we did not perform the additional high-pass filtering. We refer to the EOFs resulting from this procedure as the unfiltered-multivariate MJO indices (UMM). We then separating the UMM indices into "uniform" and "non-uniform" periods by computing the leading principle component of the UMM (PC_{M1}), and define as uniform MJO when $|PC_{M1}| \leq 0.5$ and non-uniform MJO when $|PC_{M1}| > 0.5$ (Bai et al. 2023).

c. Model and experiments

In this project, we studied the drivers of the North American Dipole (NAD) using ensemble experiment with the Community Earth System Model 2 (CESM2), a widely used and community-supported climate model developed by National Center of Atmospheric Research (NCAR) and other universities and research institutions (Danabasoglu et al. 2020). CESM2 is a fully coupled climate model consisting of atmosphere, land surface, land ice, ocean, ocean waves, river runoff, and sea ice model components, which can be dynamically linked through the central coupler which exchanges information between model components. We used a scientifically validated configuration of the model which has a prognostic atmosphere and land surface model with a prescribed ocean and sea ice state, where the Community Atmosphere Model (CAM6) used in this study provides $0.9° \times 1.25°$ (latitude/longitude) horizontal grids and 32 vertical levels. Our control runs and experiments were ensembles of thirty summers in length; we simulated only June and July for computational efficiency, discarding June as atmospheric spin-up. We note that this computational strategy will likely only produce a small spread in the land surface component over

Accepted for publication in *Journal of Climate*. DOI 10.1175/JCLI-D-23-0015.1.

a two-month period. To produce sufficient atmospheric spread in each ensemble, we perturbed the initial atmospheric temperature state following the technique used in the Large Ensemble Project (Kay et al. 2015).

In our control run, we used climatological SSTs provided with CESM2 corresponding to years 1995-2005 (Hurrell et al. 2008). Then, we conducted five experiments in which we forced CESM2 with positive and negative SST anomalies added to the climatological SSTs, taken separately and in combination over the tropical and subtropical oceans (Table 1). Two mechanisms were considered in the experiments: EAM-related convection anomalies and Rossby waves triggered by non-uniformity of the MJO phase distribution. The EAM mechanism is closely linked to SSTs by observations, and this directly informed the SST forcing regions used in the experiments (upper section of Table 1). The MJO, by contrast, interacts with SST anomalies including El Niño (Hendon et al. 2007), but is not triggered by SST anomalies per se. However, we found that we can emulate the observed seasonal-scale convection anomalies associated with non-uniform MJO (Bai et al. 2023) by prescribing positive SST anomalies below the regions of enhanced convection (lower section of Table 1, results in Section b). SST anomaly magnitudes of 0.6°C were used for the EAM mechanism to approximate the magnitude of observed anomalies, and these magnitudes were found to work well for triggering the MJO-like convection patterns.

For the EAM mechanism, our hypothesis was that the case 1 experiment with cool Southern Japan and the dipole pattern (above-averaged SST in El Niño region and below-averaged SST in South East Asian area) in the equatorial Pacific would promote strong convection over Southern Japan, resembling patterns observed during relatively high East Asian precipitation (P_{EA}). Cases 2 and 3 are a decomposition of case 1 to study how its forcing regions influence the atmosphere separately versus together. We hypothesized that cases 4 and 5 would trigger convection patterns associated with anomalously frequent MJO phases 1 and 6 and yield extratropical teleconnections which project onto the NAD.

d. Rossby wave source

In order to interpret the teleconnection between MJO and NAD, we computed the linearized Rossby wave source (RWS) for the anomaly field (Sardeshmukh and Hoskins 1988):

Accepted for publication in *Journal of Climate*. DOI 10.1175/JCLI-D-23-0015.1.

$$RWS = -\nabla \cdot (\mathbf{u}'_\chi \zeta'_a) \tag{1}$$

where $\mathbf{u}'_\chi = (u'_\chi, v'_\chi)$ is the divergent wind component, obtained from velocity potential, and ζ'_a is the vertical component of the absolute vorticity. This provides a diagnostic framework to quantify how the divergent flow, associated with the anomalous heating, leads to substantial forcing on the barotropic vorticity and acts as the RWS. We computed the fields of vorticity, horizontal divergence and the divergent wind components based on the zonal and meridional wind velocities by using a spectral expansion with T42 truncation.

Accepted for publication in *Journal of Climate*. DOI 10.1175/JCLI-D-23-0015.1.

TABLE 1. CESM experiments focused on the EAM and MJO mechanisms, where plus indicate above-averaged SST forcings (+0.6°C), minus indicates below-averaged SST forcings (−0.6°C), and 0 means climatological SST in the forcing region. The CTL column corresponds to the control run. Oceanic forcing regions (shown in Figs. 3a, 7a, and 8a) are defined as Southern Japan (25°-35°N, 120°-150°E), Southeast Asia (10°S-10°N, 90°-150°E), eastern tropical Pacific (10°S-10°N, 80°-170°W), Western Indian Ocean (10°S-10°N, 50°-70°E), Eastern Pacific (10°S-10°N, 85°-115°W), and Western Tropical Pacific area (10°S-10°N, 120°-180°E). The final row in the table reports the spatial pattern Pearson correlation between the 300-hPa geopotential height (Z_{300}) response patterns presented in results for each case and the observed NAD pattern (i.e., shading, Fig. 1c); these correlations are all statistically significant ($p < 0.01$) and were calculated over the domain mapped in Fig. 1.

Case List								
Mechanism	Oceanic forcing regions	CTL	case 1	case 2	case 3	case 4	case 5	case 6
EAM	Southern Japan	0	–	0	–	0	0	–
	Southeast Asia	0	–	–	0	0	0	0
	Eastern tropical Pacific	0	+	+	0	0	0	0
MJO	Western Indian Ocean	0	0	0	0	+	0	+
	Eastern Pacific	0	0	0	0	+	0	+
	Western Tropical Pacific	0	0	0	0	0	+	0
	NAD pattern correlation		0.49	0.42	0.23	0.54	-0.11	0.47

Accepted for publication in *Journal of Climate*. DOI 10.1175/JCLI-D-23-0015.1.

3. Result

Bai et al. (2023) defined North American dipole (NAD) as the second empirical orthogonal function (EOF2) of June-August 500-hPa geopotential height (Z_{500}) during 1950-2019 over the domain of 35°-65°N, 170°-340°E. The loading pattern of the NAD is shown as blue contour in Fig. 1c. The NAD pattern defined at 500-hPa aligns well with the upper tropospheric circulation at 300-hPa where we study simulation response patterns here. To illustrate this, we compare the Z_{300} anomalies for high and low NAD to the NAD pattern diagnosed at 500-hPa. The composite anomalies of Z_{300} for low NAD years (below 10th percentile) and high NAD years (above 90th percentile) show west-east dipoles over continental North America (Figs. 1a and b). The associated composite anomaly difference between high and low NAD years captured a prominent west-east dipole (shading, Fig. 1c) which is significantly correlated with NAD EOF loading pattern diagnosed at 500-hPa (i.e., spatial Pearson correlation between shaded and contoured fields in Fig. 1c is $r = 0.85, p < 0.001$). We use the shaded result in Fig. 1c as the observed NAD pattern and compare it to simulated response patterns using spatial Pearson correlations presented for each simulation case (Table 1).

Accepted for publication in *Journal of Climate*. DOI 10.1175/JCLI-D-23-0015.1.

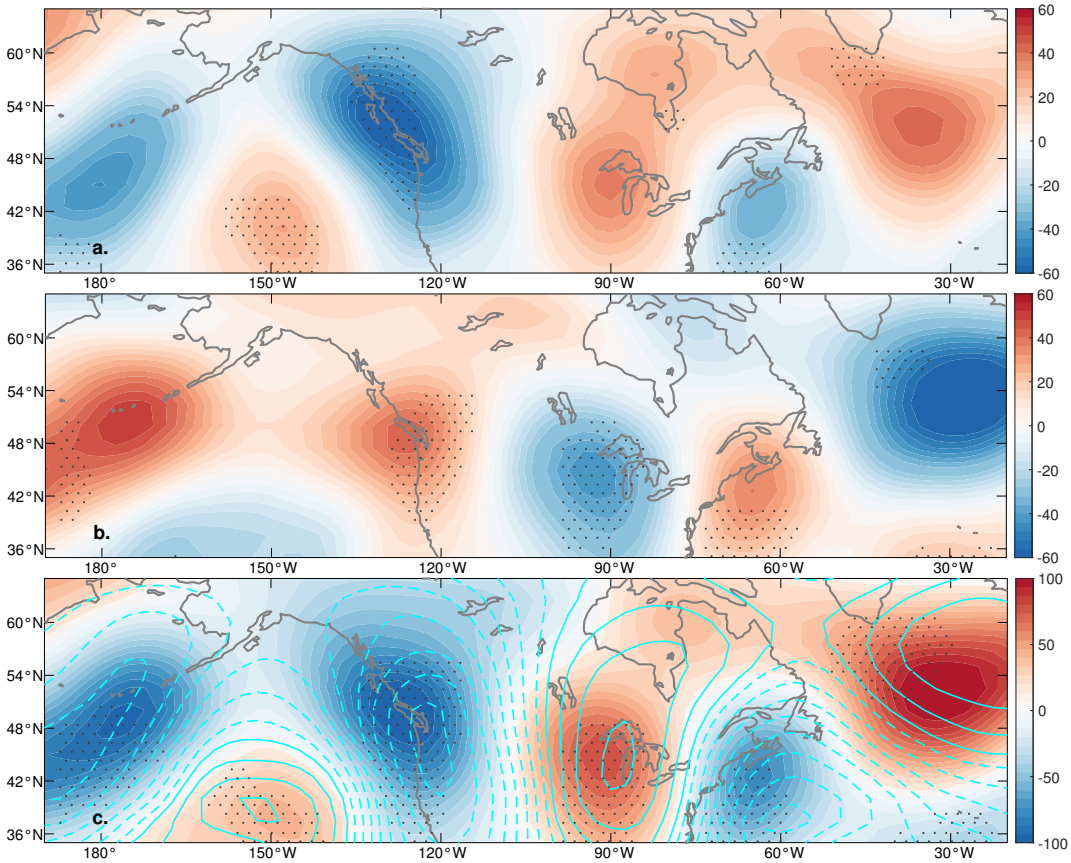

FIG. 1. Composite Z_{300} anomalies for (a) high NAD years (above 90th percentile) and (b) low NAD years (below 10th percentile), and (c) the differences between the composite Z_{300} anomalies for high and low NAD years (shading) and the loading pattern of NAD (blue contours with negative value dashed). Stippling indicates statistical significance at the 95% confidence level, the analysis period is 1950-2019, and the pattern is presented over the NAD domain (35°-65°N, 170°-340°E).

a. Role of Southern Japan convection (EAM mechanism)

We begin by highlighting some observational results related to our prior work (Bai et al. 2023) that have specific relevance to the experiment results presented in this study. The correlation of SST with P_{EA} features distinct dipoles over Southern Japan region and the equatorial Pacific both in climatological summer (June-August, JJA) (Fig. 2a) and July alone (Fig. 2b). The ENSO-ike equatorial SST results are clearest during July when the correlations become broadly significant (Fig. 2b). Considering the overall strength of the July-only SST pattern, we focus our experimental

Accepted for publication in *Journal of Climate*. DOI 10.1175/JCLI-D-23-0015.1.

design on July (i.e., simulations are run for June and July, discarding the former as spin-up as detailed in Section 2). The associated wave pattern observed on the 300-hPa pressure level (Z_{300}) depicted a pan-Pacific circulation completing one to two wave cycles over the North Pacific (Figs. 2c and 2d), showing anomalously low heights over western North America and anomalously high heights over eastern North America. This dipole structure in the height anomalies is a driver of the west-east mode of Pine Siskin migration in the boreal forest (Strong et al. 2015; Bai et al. 2023).

In our experimental framework, modulating precipitation over Southern Japan enabled us to study pan-Pacific Rossby waves of potential importance to the NAD. In case 1, we combined the cool Southern Japan SST forcing with the the El Niño-like (cool southeast Asia and warm tropical Pacific) dipole pattern (Table 1). The case 1 forcing regions are indicated by blue and red boxes in Fig. 3a, where the blue box indicates cool SST forcing (−0.6°C) and the red box indicates warm SST forcing (+0.6°C). The model results depicted a negative OLR anomaly and a positive precipitation anomaly over the East China Sea region (Figs. 3a and 3c), consistent with enhanced convection over southern Japan. In addition, the El Niño-like dipole pattern triggered significant suppression of convection over the South China Sea and deep convection over the central tropical Pacific, which favored the formation of the upper-level zonally elongated height anomalies over Japan and the North Pacific with a NAD signature downstream over North America (Fig. 3b). The spatial correlation between the observed and simulated NAD patterns (i.e., Figure 3b and Fig. 1c) over the domain in the latter is $r = 0.49$ with $p < 0.01$ (Table 1).

The experiment with only El Niño-like SST forcing (case 2, Table 1) produced suppressed convection over the Maritime Continent and enhanced convection over the eastern tropical Pacific region (Fig. 4a), consitent with decreased precipitation over the western tropical Pacific and increased precipitation over the eastern tropical Pacific (Fig. 4c). The associated geopotential height response resembled the NAD as part of the summer east Atlantic (SEA) pattern (Fig. 4b), where SEA is triggered by a warm Pacific-Caribbean SST dipole with a distinct upper-level quadpole over the eastern North America-western Europe (Wulff et al. 2017). The spatial correlation between the observed and simulated NAD patterns (i.e., Figure 4b and Fig. 1c) over the domain in the latter is $r = 0.42$ with $p < 0.01$ (Table 1).

Further decomposing the SST forcing regions in the EAM mechanism, case 3 examines the effect of the negative SST anomaly in the Southern Japan region alone (Table 1). The position

Accepted for publication in *Journal of Climate*. DOI 10.1175/JCLI-D-23-0015.1.

of the negative SST anomaly in case 3 (blue box, Fig. 5a) produced the desired wet-dry dipole over Indonesia and the east China Sea area (Fig. 5c). The associated Z_{300} anomalies lined up well with the observational analysis showing a pan-Pacific wave over the Northern Pacific connected to a downstream NAD signature (Fig. 5b). Overall, the upper-level wave structure was similar in cases 1 and 3, indicating that cool-Japan only SST forcing can produce the heavy rainfall over east Asia which initiates the pan-Pacific Rossby wave associated with the NAD. Contrasting case 3 with cases 1 and 2, the tropical El Niño-like SST pattern deepened the zonally elongated trough over East Asia and the North Pacific. It is also interesting that the a similar, possibly CGT-like, continental-scale tripole pattern appears over Eurasia in all three cases (Figs. 3-5). The spatial correlation between the observed and simulated NAD patterns (i.e., Figure 5b and Fig. 1c) over the domain in the latter is a relatively modest $r = 0.23$ with $p < 0.01$ (Table 1).

Accepted for publication in *Journal of Climate*. DOI 10.1175/JCLI-D-23-0015.1.

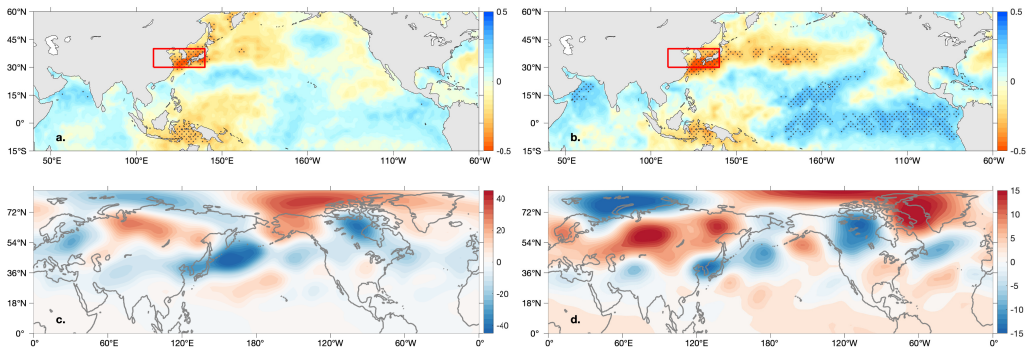

FIG. 2. Correlation of P_{EA} with HadISST sea surface temperature in (a) June-August (JJA) and (b) July only, where stippling indicates significance at the 95% confidence level based on a *t*-test assuming one degree of freedom per year and the red box indicates the averaging region for P_{EA}. Composite NCEP/NCAR Z_{300} anomalies in July for (c) relatively high P_{EA} (above 85th percentile) and (d) above-average P_{EA}. The analysis period is 1950-2019.

Accepted for publication in *Journal of Climate*. DOI 10.1175/JCLI-D-23-0015.1.

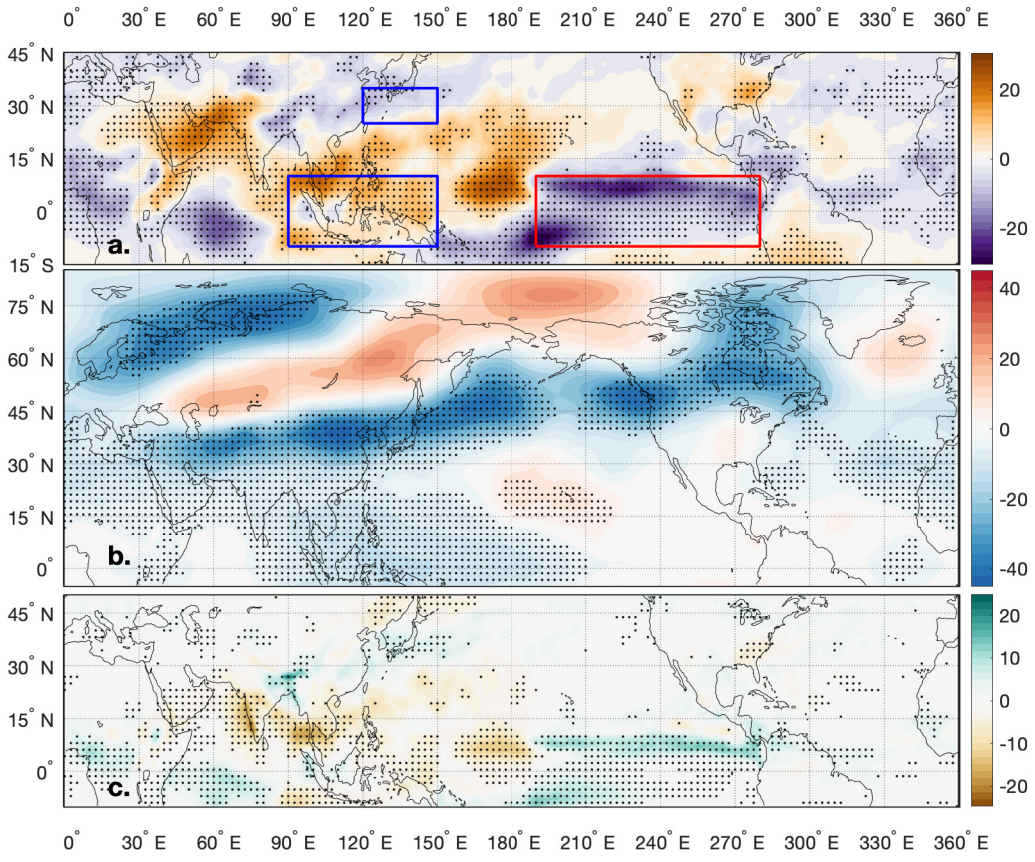

FIG. 3. For experiment case 1, anomalies of July (a) OLR (W m^{-2}), (b) Z_{300} (m), and (c) total precipitation (mm). Boxes indicate SST forcing regions given in Table 1 case 1, where the blue box indicates a −0.6°C forcing region and the red box indicates a +0.6°C forcing region. Stippling indicates statistical significance at the 95% confidence level based on a *t*-test assuming one degree of freedom per ensemble member.

Accepted for publication in *Journal of Climate*. DOI 10.1175/JCLI-D-23-0015.1.

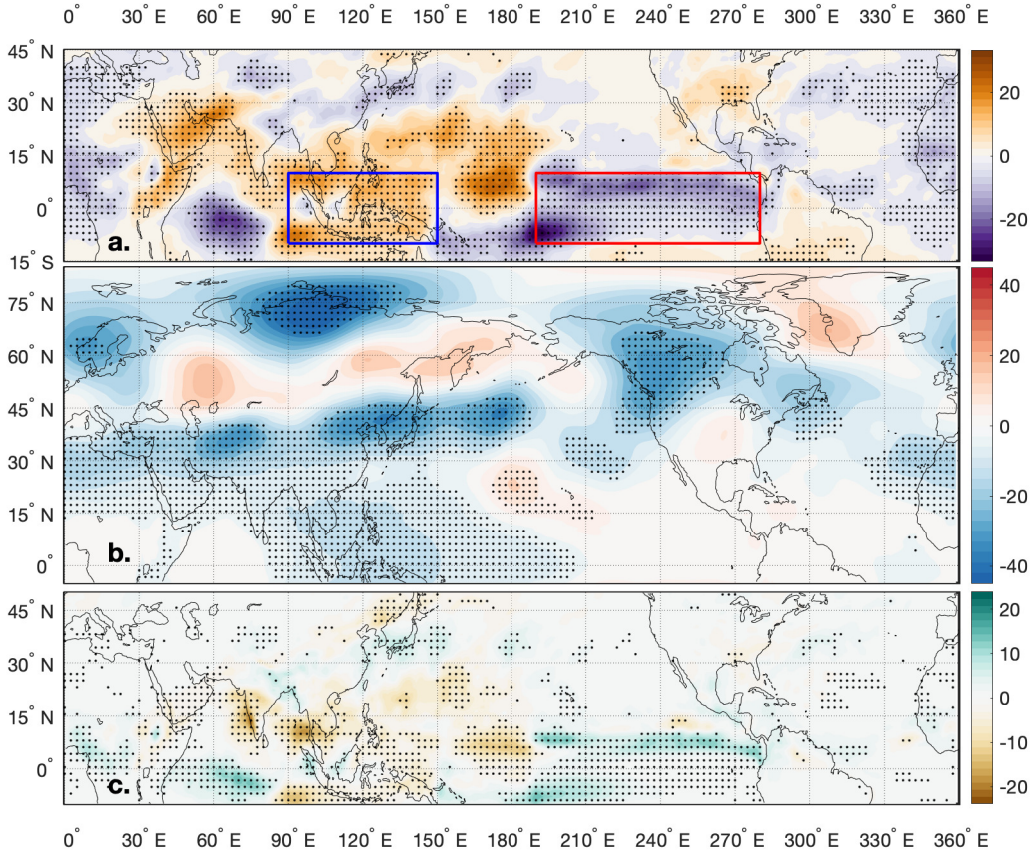

FIG. 4. Same as Fig. 3 but for experiment case 2.

Accepted for publication in *Journal of Climate*. DOI 10.1175/JCLI-D-23-0015.1.

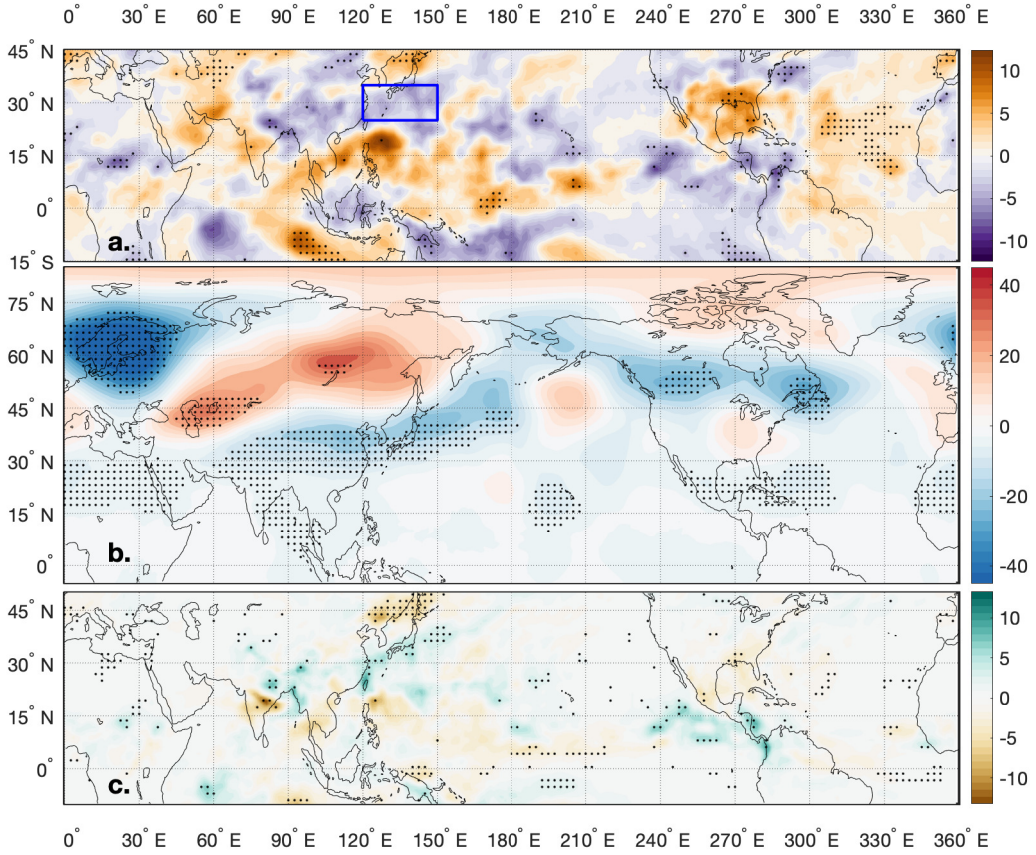

FIG. 5. Same as Fig. 3 but for experiment case 3.

Accepted for publication in *Journal of Climate*. DOI 10.1175/JCLI-D-23-0015.1.

b. Role of tropical convection (non-uniform MJO mechanism)

To clarify the motivation for our experimental design related to MJO, we offer some observational results and remarks on the associated timescales. Although MJO as conventionally defined has inherently subseasonal timescales, its aggregate effects to project onto and exhibit lower frequency variability (Wang et al. 2021; Dasgupta et al. 2021; Bai et al. 2023). First considering seasonal observations, MJO phase 1 featuring negative OLR anomalies over the tropical western Indian Ocean and eastern Pacific Ocean (contours, Fig. 6a). The associated extratropical height anomaly pattern indicates a positive NAD (shading, Fig. 6a). Associated patterns based on MJO phase 6 are essentially opposite to the phase 1 results, featuring a reversed tropical OLR pattern with negative NAD (Fig. 6b). Bridging to lower frequencies, Bai et al. (2023) found an MJO mechanism related to anomalously frequent occurrence of MJO phases 1 or 6 over a three-month period (May-July), which was captured by the leading principal component of the phase distribution of daily MJO (PC_{M1}; accounting for 46% of the phase variance). In summers when this MJO nonuniformity was active, positive NAD was strongly linked to anomalously frequent MJO phase 1. Illustrating this, the spatial pattern of the NAD (Fig. 1c) is significantly correlated with the composite Z_{300} anomaly pattern for high PC_{M1} (Fig. 6a) ($r = 0.49, p < 0.001$ calculation over the NAD domain). Similarly, the spatial pattern of the NAD (Fig. 1c) is significantly negatively correlated with the composite Z_{300} anomaly pattern for low PC_{M1} (Fig. 6b) ($r = -0.46, p < 0.001$; calculation over the NAD domain).

Our objective is thus to investigate how the above-described convection patterns associated with anomalously frequent MJO phase 1 or 6 affect the extratropical circulation when aggregated to monthly or longer timescales. Importantly, our aim is not to simulate the MJO itself, which would require careful attention to diabatic heating profiles, SST specification, and possibly ocean coupling (Lappen and Schumacher 2012, and references therein). Instead, we simply want to trigger monthly-to-seasonal convection anomaly patterns resembling those observed with anomalously frequent MJO phase 1 or 6 (Bai et al. 2023), and we found here that we can accomplish this by prescribing positive SST anomalies below the regions of enhanced convection (lower section of Table 1). This simulation strategy exploits the diabatic heating that fundamentally arises from SST forcing (e.g., Webster 1981), and of course in no way implies that the MJO is SST-triggered [although the MJO does interact with SST patterns including ENSO (Hendon et al. 2007)].

Accepted for publication in *Journal of Climate*. DOI 10.1175/JCLI-D-23-0015.1.

To simulate the MJO phase 1 pattern in Fig. 6a, our case 4 experiment imposed +0.6°C SST anomalies below two regions where observed OLR indicated enhanced convection (red boxes, Fig. 7a; Table 1). This forcing triggered significant negative OLR anomalies over both forcing regions, and the spatial Pearson correlation between the simulated OLR pattern (Fig. 7a) and observed OLR pattern (Fig. 6a) was $r = 0.44$ ($p < 0.01$). The associated Z_{300} anomaly pattern captured the pan-Pacific Rossby wave associated with the positive NAD (Fig. 7b). The spatial Pearson correlation between the observed NAD (Fig. 1c) and the simulated height response (Fig. 7b) was $r = 0.54$ ($p < 0.01$; Table 1). Notably, the upper-level wave patterns in both modeling and observational analyses showed strong agreement on the midlatitude Rossby wave train over the Northern Hemisphere, indicating a tropical-extratropical teleconnection associated with anomalously frequent MJO phase 1 featuring intensified convection over the Indian Ocean. Similar teleconnection patterns have been reported in prior work on the cicumglobal teleconnection (CGT) pattern during boreal summer, which is closely associated with Indian summer monsoon variability (Ding et al. 2011).

To simulate the MJO phase 6 pattern in Fig. 6b, our case 5 experiment imposed +0.6°C SST anomalies below the western tropical Pacific region where observed OLR indicated enhanced convection (red box, Fig. 8a; Table 1). This forcing triggered a significant negative OLR anomaly over the western north Pacific region indicating deep convection and heavy rainfall over this area (Fig. 8a), and the spatial Pearson correlation between the simulated OLR pattern (Fig. 8a) and observed OLR pattern (Fig. 6b) was $r = 0.58$ ($p < 0.01$). Additionally, the associated upper-level height anomalies in the model result lined up with observational analyses appearing as a wave train initiated from near Indonesia and propagating northward and eastward toward western North America (Fig. 8b), confirming that MJO-like convection anomalies can force NAD-like Northern Hemisphere extratropical response patterns. It also shows the tight relationship between western Pacific convection and the NAD by revealing the chain of cyclonic and anticyclonic anomalies from the upstream subtropical area to the mid-latitudes of northern Japan, the Okhotsk Sea, and downstream North America. However, the spatial Pearson correlation between the observed NAD (Fig. 1c) and the simulated height response (Fig. 8b) was weak ($r = -0.11$, $p < 0.01$; Table 1). We note that the negative sign is expected here because anomalously frequent MJO phase 6 is associated with negative NAD by prior work (Bai et al. 2023).

Accepted for publication in *Journal of Climate*. DOI 10.1175/JCLI-D-23-0015.1.

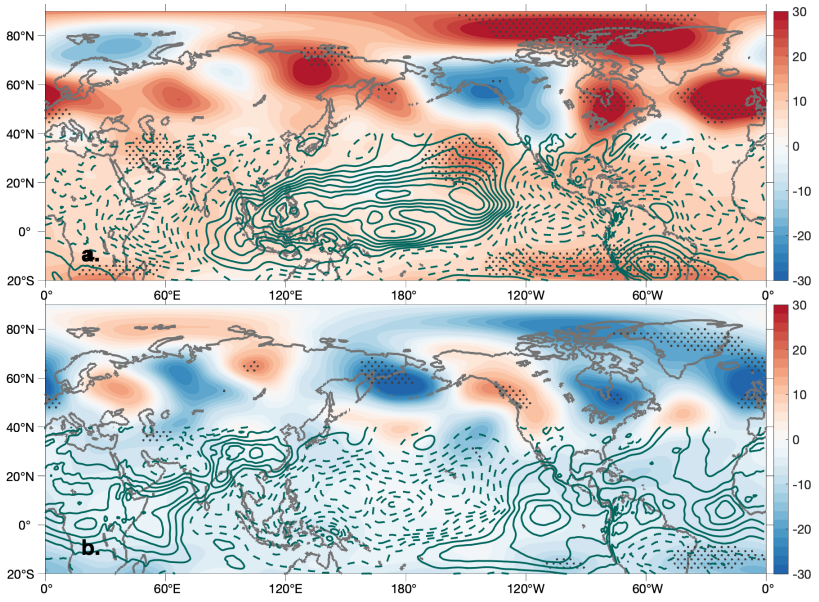

FIG. 6. Composite anomalies of June-July Z_{300} (shading, m) and OLR (contoured at 2 Wm^{-2} with negative values dashed and zero contour suppressed) for (a) high PC_{M1} years (above 90th percentile) and (b) low PC_{M1} years (below 10th percentile), where PC_{M1} indicates the leading principle component of daily UMM defined by Bai et al. (2023).

Accepted for publication in *Journal of Climate*. DOI 10.1175/JCLI-D-23-0015.1.

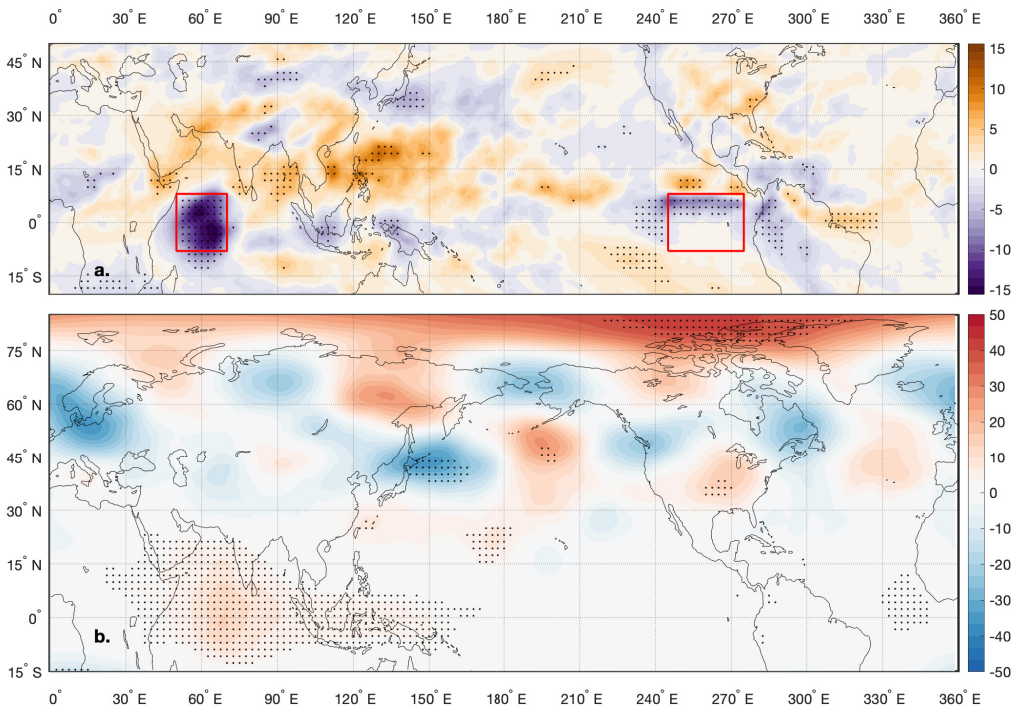

FIG. 7. For experiment case 4, anomalies of July (a) OLR (W m^{-2}) and (b) Z_{300} (m). The boxes indicates the +0.5°C SST forcing regions given in Table 1 case 4, and stippling indicates statistical significance at the 95% confidence level based on a *t*-test assuming one degree of freedom per ensemble member.

Accepted for publication in *Journal of Climate*. DOI 10.1175/JCLI-D-23-0015.1.

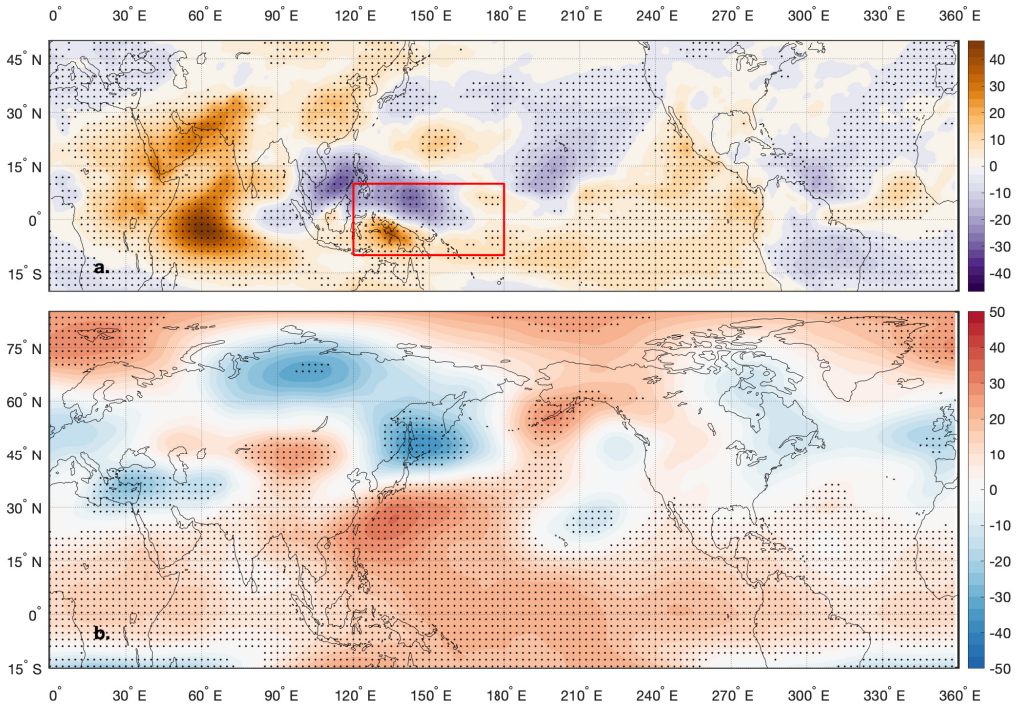

FIG. 8. As in Fig. 3 but for experiment case 5.

Accepted for publication in *Journal of Climate*. DOI 10.1175/JCLI-D-23-0015.1.

c. Rossby wave source analysis

To further interpret the teleconnections found in the EAM mechanism and MJO mechanism experiments, we show the Rossby wave source (RWS) and divergent wind for cases 3 (EAM) and case 4 (MJO phase 1) at 850-hPa and 250-hPa in Fig. 9. In this framework, positive and negative RWS correspond to an increasing tendency of cyclonic or anticyclonic vorticity, respectively. For EAM, the simulated wet-south / dry-north precipitation anomaly over Japan (Fig. 4c) is logically aligned with a positive-south / negative-north RWS dipole at 850-hPa over Japan (Fig. 9a). Ascending motion over the positive RWS is associated with an overlying negative RWS and divergence at 250-hPa, with the reverse pattern to its north (Fig. 9b). For MJO phase 1 (the case 4 experiment), RWS analysis indicated lower-level convergence and upper-level divergence over the SST forcing domain (red box; Figs. 9c, d), supporting the indication from observations and model experiments that deep convection over the tropical Indian Ocean can trigger the teleconnection pattern leading to NAD.

d. Tropical and monsoonal convection

A one-point correlation map for Z_{300} using the NAD's western center of action as the origin yields a pan-Pacific Rossby wave pattern (Fig. 10a), whereas a one-point correlation map for Z_{300} using the NAD's eastern center of action as the origin yields a Rossby wave from the central tropical Pacific which is very similar to the non-uniform MJO teleconnection pattern (Fig. 10b). This historical observational result agrees well with the result in experiment case 6 (Fig. 11), showing that enhanced convection and increased precipitation over both East Asia and the western Indian and eastern Pacific Oceans can produce NAD-like circulation patterns. The spatial Pearson correlation between the observed NAD (Fig. 1c) and the simulated height response (Fig. 11b) was $r = 0.$ ($p < 0.01$; Table 1). This supports the interpretation that the NAD is a superposition of two standing Rossby waves – one triggered by EAM convection in a pattern most apparent in uniform MJO summers and one triggered by anomalies in the seasonal phase distribution of the MJO most apparent in non-uniform MJO summers as discussed in prior observational work (Bai et al. 2023).

Accepted for publication in *Journal of Climate*. DOI 10.1175/JCLI-D-23-0015.1.

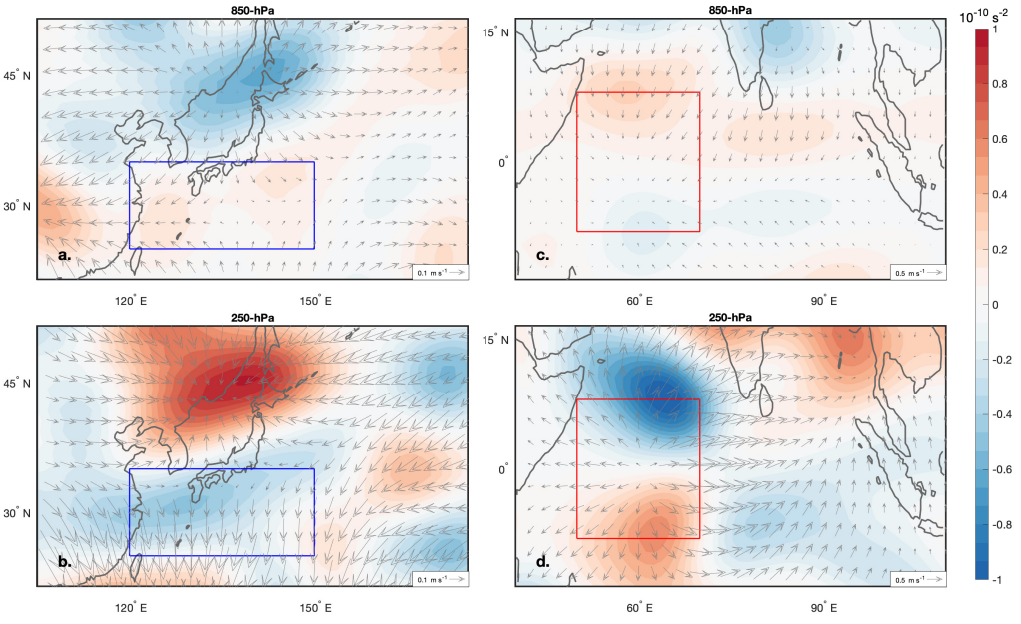

FIG. 9. Rossby wave source (shading) and divergent wind (vector) for case 3 at (a) 850-hPa and (b) 250-hPa. (c-d) Same as (a,b) but for case 4. Boxes indicate the respective SST forcing regions (Table 1).

Accepted for publication in *Journal of Climate*. DOI 10.1175/JCLI-D-23-0015.1.

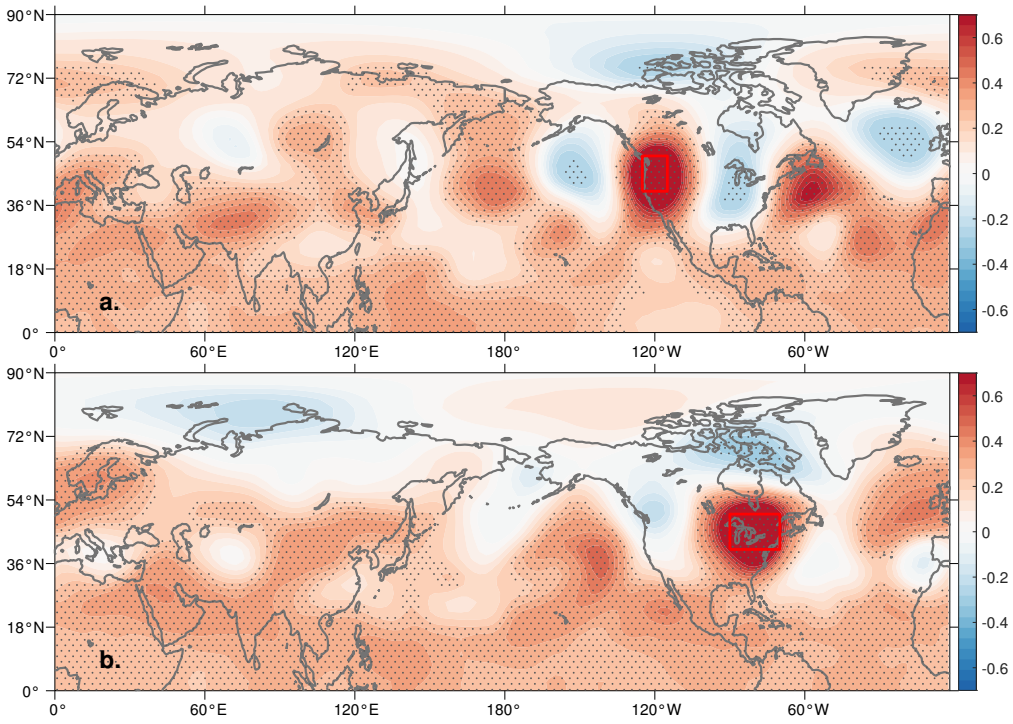

FIG. 10. One-point correlation maps of July Z_{300} with (a) Z_{300} averaged over the Pacific Northwest (red box) and (b) Z_{300} averaged over eastern North America (red box) based on the NCEP/NCAR reanalysis. Stippling indicate statistical significance at the 95% confidence level, data were detrended, and the analysis period is 1950-2019.

Accepted for publication in *Journal of Climate*. DOI 10.1175/JCLI-D-23-0015.1.

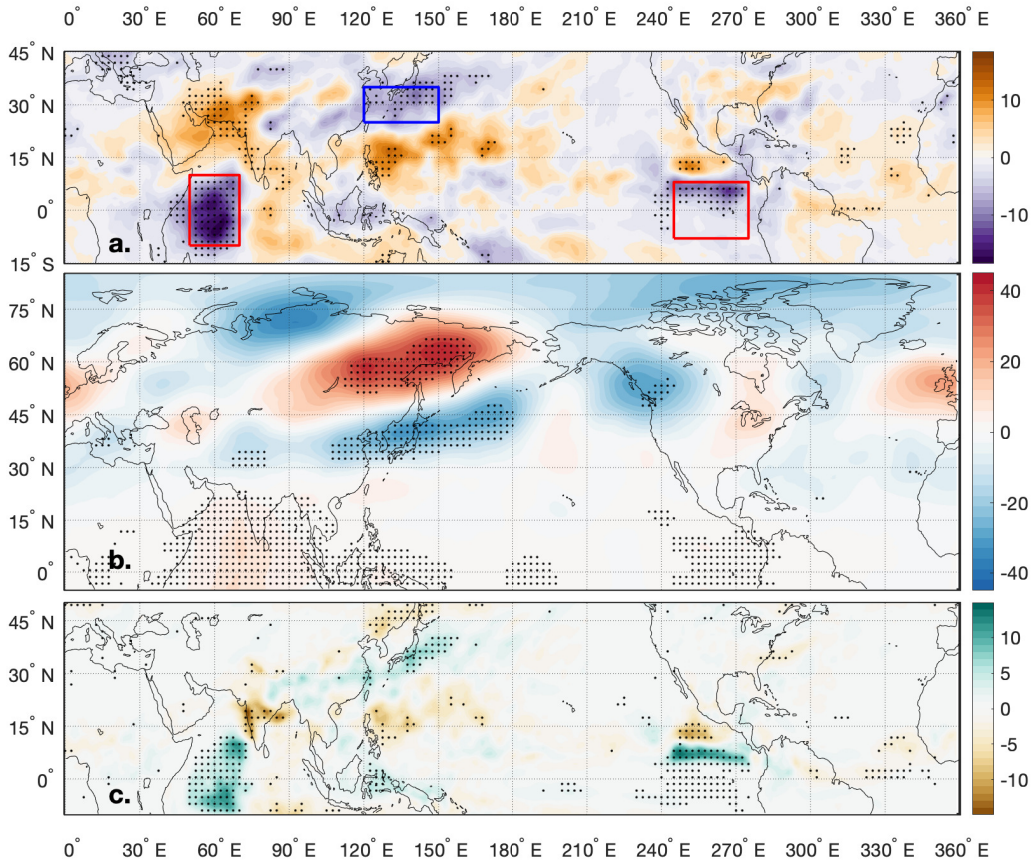

FIG. 11. Same as Fig. 3 but for experiment with case 6.

Accepted for publication in *Journal of Climate*. DOI 10.1175/JCLI-D-23-0015.1.

4. Discussion and conclusion

Observational correlations and composites indicated two teleconnection mechanisms through which convection can trigger the NAD, the first related to P_{EA} anomalies associated with EAM convection and the second stemming from anomalies in the phase distribution of the MJO. Atmospheric boundary forcing experiments were conducted with CESM2 in which we used SST anomalies to trigger convection patterns observed during high P_{EA} as well as anomalously frequent MJO phases 1 and 6. The spatial pattern correlation between the simulated 300-hPa geopotential height response patterns for each case and the empirical orthogonal function (EOF) defining the observed NAD (Bai et al. 2023) was statistically significant ($p < 0.001$) for all six experiment cases (lower row, Table 1). In interpreting these correlations, note that the negative sign for case 5 is logical because the associated forcing produced convection patterns associated with anomalously frequent MJO phase 6.

Model results showed that a cool-Southern Japan forcing with an El Niño-like tropical pattern (case 1, Table 1) successfully generated zonally elongated height anomalies over the Pacific-Japan sector, leading to a downstream cyclonic anomaly over the western Canada and anticyclonic anomaly over the Appalachian region (Fig. 3b), in agreement with the conditions observed during high P_{EA} and positive NAD (Fig. 2c). Interestingly, the case 2 parallel experiment removing the cool Japan forcing (Fig. 4) showed that the response to an El Niño-like SST pattern resembles NAD as part of the SEA pattern through modulating the upper-level ridge and trough over eastern North America and the eastern Atlantic (Wulff et al. 2017; Sardeshmukh and Hoskins 1988). The case 3 simulation using only the cool Japan forcing without ENSO was able to capture some aspects of the observed NAD pattern, namely enhanced convection over southern Japan with a pan-Pacific wave train leading to a positive NAD-like pattern over North America, further supporting the observed association between the NAD and above-average P_{EA} (Fig. 2d).

Deep convection near Japan is a commonly discussed mechanism for triggering pan-Pacific teleconnections (Lau and Weng 2002), and our findings on the NAD add to this body of work. Our findings indicate that P_{EA} anomalies play a significant role in the pan-Pacific circulation (Fig. 3 and Fig. 5) as seen in prior results, highlighting the impact of the Pacific-Japan (PJ) pattern on upper-level wave activity from the western Pacific to the west coast of the North America (Nitta 1987; Kosaka and Nakamura 2008).

Accepted for publication in *Journal of Climate*. DOI 10.1175/JCLI-D-23-0015.1.

Prior work shows that the leading mode of variability in unfiltered MJO phase captures the tendency for phase 1 or 6 to occur anomalously frequently, and the associated convection anomalies are associated with extratropical signatures resembling the NAD (Bai et al. 2023). We examined the MJO phase 1 and phase 6 teleconnection in the case 4 and 5 model experiments by using anomaloulsy high SSTs to trigger the associated convective patterns. The simulation results support the observational analyses, with response patterns resembling positive NAD in the MJO phase 1 experiment (case 4; Fig. 7b) and negative NAD in the MJO phase 6 experiment (case 5; Fig. 8b). These results are also consistent with prior research showing that anomalous heating over the Indian Ocean and the western Pacific impacts the dipole-like Rossby wave pattern over the Gulf of Alaska and western North America (Tseng et al. 2019). Moreover, the MJO phase 1 simulation indicated that the Indian Ocean convective activity plays a contributing role in the pan-Pacific wave train, which is in line with studies showing the importance of the Indian Summer Monsoon in driving the summertime circumglobal teleconnection (Branstator 2002; Ding and Wang 2005). The MJO phase 6 simulation indicated the significant influence of western Pacific convection on the NAD, which is consistent with previous work identifying the western north Pacific summer monsoon as an important contributor to the West Pacific-North American wave pattern (Ding et al. 2011).

Here, we reconstructed the convective activity similar to the MJO phase 1 and 6 by forcing SST over the associated tropical regions. Future work also can consider applying diabatic heating anomalies over the MJO phase 1 and 6 regions to produce the corresponding convective patterns, following methods aimed specifically at simulating the MJO per se (Lappen and Schumacher 2012). It may also be useful to extend this study to incorporate a slab model or fully coupled framework to under potentially important impacts from atmosphere-ocean coupling (Sun et al. 2022).

To compare simulations to observations, we defined the NAD pattern as the Z_{300} pattern in high-NAD years minus low-NAD years. The spatial correlation between this observed NAD and the model circulation patterns over the NAD domian were all statistically significant at $p < 0.01$. The pattern match in case 1 was slightly higher than the case 2 and 3, indicating that both southern Japan and ENSO-like tropical convection influence the monsoonal precipitation which triggers the NAD. Furthermore, case 4 showed the strongest pattern match ($r = 0.54$, Table 1), meaning that western Indian Ocean convection has an important influence on the NAD via Rossby wave

Accepted for publication in *Journal of Climate*. DOI 10.1175/JCLI-D-23-0015.1.

propagation. These simulations suggest that the southern Japan SST forcing region has a secondary importance in triggering the NAD. It produced only a somewhat NAD-like pattern by itself (case 3), and only slightly improved the NAD produced by ENSO-like forcing (case 1 versus 2). The southern Japan forcing also had a slight negative impact on the NAD produced by the OLR forcing associated with anomalously frequent MJO phase 1 (case 6 versus 4).

Considering prior observational work together with the simulation results presented here, we conclude that The NAD is driven by stationary Rossby wave triggered by tropical and monsoonal convection anomalies. Specifically, NAD's western center links significantly to the anomalously high precipitation over east Asia and the eastern center links to the MJO phase 1-like convection pattern. In future work, it could be interesting to use a fully coupled modeling framework and longer integrations to investigate how the circulation response may depend on feedback from the ocean.

Accepted for publication in *Journal of Climate*. DOI 10.1175/JCLI-D-23-0015.1.

Acknowledgments. This project was supported by National Science Foundation award 1926221. We thank the University of Utah Center for High Performance Computing (CHPC) for computational resources and computer-support services. We also thank the editor and three anonymous reviewers for their feedback and comments to improve the manuscript.

Data availability statement. Atmospheric field data used in this ressearch are available from the European Centre for Medium Range Weather Forecasts (ECMWF) Reanalysis (ERA5) (`https://www.ecmwf.int/en/forecasts/datasets/reanalysis-datasets/era5`) and NOAA PSL's 20th Century Reanalysis (`https://psl.noaa.gov/data/`). Sea surface temperature is from the Hadley Centre Sea Ice and Sea Surface Temperature dataset at `https://www.metoffice.gov.uk/hadobs/hadsst2/`. The output data from community earth system model (CESM) simulations are available upon request.

References

Alexander, M. A., I. Bladé, M. Newman, J. R. Lanzante, N.-C. Lau, and J. D. Scott, 2002: The atmospheric bridge: The influence of ENSO teleconnections on air–sea interaction over the global oceans. *Journal of Climate*, **15 (16)**, 2205 – 2231, https://doi.org/10.1175/1520-0442(2002)015⟨2205:TABTIO⟩2.0.CO;2.

Alexander, M. A., N.-C. Lau, and J. D. Scott, 2004: Broadening the atmospheric bridge paradigm: ENSO teleconnections to the tropical west Pacific-Indian oceans over the seasonal cycle and to the North Pacific in summer. *Earth's Climate: The Ocean-Atmosphere Interaction, Geophys. Monogr*, **147**, 85–103.

Bai, H., C. Strong, and B. Zuckerberg, 2023: Drivers of an ecologically relevant summer north american dipole. *Journal of Climate*, **36 (8)**, 2387 – 2399, https://doi.org/https://doi.org/10.1175/JCLI-D-22-0542.1, URL https://journals.ametsoc.org/view/journals/clim/36/8/JCLI-D-22-0542.1.xml.

Branstator, G., 2002: Circumglobal Teleconnections, the Jet Stream Waveguide, and the North Atlantic Oscillation. *Journal of Climate*, **15 (14)**, 1893 – 1910, https://doi.org/10.1175/1520-0442(2002)015⟨1893:CTTJSW⟩2.0.CO;2, URL https://journals.ametsoc.org/view/journals/clim/15/14/1520-0442_2002_015_1893_cttjsw_2.0.co_2.xml.

Accepted for publication in *Journal of Climate*. DOI 10.1175/JCLI-D-23-0015.1.

Cassou, C., C. Deser, L. Terray, J. W. Hurrell, and M. Drévillon, 2004: Summer sea surface temperature conditions in the North Atlantic and their impact upon the atmospheric circulation in early winter. *Journal of Climate*, **17 (17)**, 3349 – 3363, https://doi.org/10.1175/1520-0442(2004)017⟨3349:SSSTCI⟩2.0.CO;2.

Compo, G. P., J. S. Whitaker, and P. D. Sardeshmukh, 2006: Feasibility of a 100-year reanalysis using only surface pressure data. *Bulletin of the American Meteorological Society*, **87 (2)**, 175–190, https://doi.org/https://www.jstor.org/stable/26233278.

Danabasoglu, G., and Coauthors, 2020: The community earth system model version 2 (CESM2). *Journal of Advances in Modeling Earth Systems*, **12 (2)**, https://doi.org/10.1029/2019MS001916.

Dasgupta, P., M. Roxy, R. Chattopadhyay, C. Naidu, and A. Metya, 2021: Interannual variability of the frequency of MJO phases and its association with two types of ENSO. *Scientific reports*, **11 (1)**, 1–16, https://doi.org/https://doi.org/10.1038/s41598-021-91060-2.

Ding, Q., and B. Wang, 2005: Circumglobal teleconnection in the northern hemisphere summer. *Journal of Climate*, **18 (17)**, 3483 – 3505, https://doi.org/10.1175/JCLI3473.1.

Ding, Q., B. Wang, J. M. Wallace, and G. Branstator, 2011: Tropical–extratropical teleconnections in boreal summer: Observed interannual variability. *Journal of Climate*, **24 (7)**, 1878 – 1896, https://doi.org/10.1175/2011JCLI3621.1.

Hendon, H. H., M. C. Wheeler, and C. Zhang, 2007: Seasonal Dependence of the MJO–ENSO Relationship. *Journal of Climate*, **20 (3)**, 531 – 543, https://doi.org/10.1175/JCLI4003.1, URL https://journals.ametsoc.org/view/journals/clim/20/3/jcli4003.1.xml.

Horel, J. D., and J. M. Wallace, 1981: Planetary-scale atmospheric phenomena associated with the southern oscillation. *Monthly Weather Review*, **109 (4)**, 813 – 829, https://doi.org/10.1175/1520-0493(1981)109⟨0813:PSAPAW⟩2.0.CO;2.

Hurrell, J. W., J. J. Hack, D. Shea, J. M. Caron, and J. Rosinski, 2008: A new sea surface temperature and sea ice boundary dataset for the community atmosphere model. *Journal of Climate*, **21 (19)**, 5145 – 5153, https://doi.org/https://doi.org/10.1175/2008JCLI2292.1, URL https://journals.ametsoc.org/view/journals/clim/21/19/2008jcli2292.1.xml.

Accepted for publication in *Journal of Climate*. DOI 10.1175/JCLI-D-23-0015.1.

Kalnay, E., and Coauthors, 1996: The NCEP/NCAR 40-year reanalysis project. *Bulletin of the American meteorological Society*, **77 (3)**, 437–472.

Kay, J. E., and Coauthors, 2015: The community earth system model (CESM2) large ensemble project: A community resource for studying climate change in the presence of internal climate variability. *Bulletin of the American Meteorological Society*, **96 (8)**, 1333–1349, https://doi.org/10.1175/BAMS-D-13-00255.1.

Kessler, W. S., 2001: EOF representations of the Madden–Julian Oscillation and its connection with ENSO. *Journal of Climate*, **14 (13)**, 3055 – 3061, https://doi.org/10.1175/1520-0442(2001)014⟨3055:EROTMJ⟩2.0.CO;2.

Kosaka, Y., and H. Nakamura, 2006: Structure and dynamics of the summertime Pacific–Japan teleconnection pattern. *Quarterly Journal of the Royal Meteorological Society*, **132 (619)**, 2009–2030, https://doi.org/10.1256/qj.05.204.

Kosaka, Y., and H. Nakamura, 2008: A comparative study on the dynamics of the Pacific-Japan (PJ) teleconnection pattern based on reanalysis datasets. *SOLA*, **4**, 9–12, https://doi.org/10.2151/sola.2008-003.

Kosaka, Y., and H. Nakamura, 2010: Mechanisms of meridional teleconnection observed between a summer monsoon system and a subtropical anticyclone. part I: The Pacific–Japan pattern. *Journal of Climate*, **23 (19)**, 5085 – 5108, https://doi.org/10.1175/2010JCLI3413.1.

Lappen, C.-L., and C. Schumacher, 2012: Heating in the tropical atmosphere: what level of detail is critical for accurate MJO simulations in GCMs? *Climate Dynamics*, **39 (9)**, 2547–2568, https://doi.org/10.1007/s00382-012-1327-y, URL https://doi.org/10.1007/s00382-012-1327-y.

Lau, K.-M., and H. Weng, 2002: Recurrent teleconnection patterns linking summertime precipitation variability over east asia and north america. *Journal of the Meteorological Society of Japan. Ser. II*, **80 (6)**, 1309–1324, https://doi.org/10.2151/jmsj.80.1309.

Liebmann, B., and C. A. Smith, 1996: Description of a complete (interpolated) outgoing longwave radiation dataset. *Bulletin of the American Meteorological Society*, **77 (6)**, 1275–1277.

Accepted for publication in *Journal of Climate*. DOI 10.1175/JCLI-D-23-0015.1.

Matthews, A. J., 2004: Intraseasonal variability over tropical Africa during northern summer. *Journal of Climate*, **17 (12)**, 2427 – 2440, https://doi.org/10.1175/1520-0442(2004)017⟨2427:IVOTAD⟩2.0.CO;2.

Matthews, A. J., B. J. Hoskins, and M. Masutani, 2004: The global response to tropical heating in the madden–julian oscillation during the northern winter. *Quarterly Journal of the Royal Meteorological Society*, **130 (601)**, 1991–2011, https://doi.org/10.1256/qj.02.123.

Namias, J., 1976: Some statistical and synoptic characteristics associated with El Niño. *Journal of Physical Oceanography*, **6 (2)**, 130 – 138, https://doi.org/10.1175/1520-0485(1976)006⟨0130:SSASCA⟩2.0.CO;2.

Nitta, T., 1987: Convective activities in the tropical western Pacific and their impact on the Northern Hemisphere summer circulation. *Journal of the Meteorological Society of Japan. Ser. II*, **65 (3)**, 373–390, https://doi.org/10.2151/jmsj1965.65.3_373.

Palmer, T. N., and S. Zhaobo, 1985: A modelling and observational study of the relationship between sea surface temperature in the north-west atlantic and the atmospheric general circulation. *Quarterly Journal of the Royal Meteorological Society*, **111 (470)**, 947–975, https://doi.org/10.1002/qj.49711147003.

Sardeshmukh, P. D., and B. J. Hoskins, 1988: The generation of global rotational flow by steady idealized tropical divergence. *Journal of Atmospheric Sciences*, **45 (7)**, 1228 – 1251, https://doi.org/10.1175/1520-0469(1988)045⟨1228:TGOGRF⟩2.0.CO;2.

Strong, C., B. Zuckerberg, J. L. Betancourt, and W. D. Koenig, 2015: Climatic dipoles drive two principal modes of north american boreal bird irruption. *Proceedings of the National Academy of Sciences*, **112 (21)**, E2795–E2802, https://doi.org/10.1073/pnas.1418414112.

Sun, X., and Coauthors, 2022: Enhanced jet stream waviness induced by suppressed tropical pacific convection during boreal summer. *Nature Communications*, **13 (1)**, 1288.

Thomson, S. I., and G. K. Vallis, 2018: Atmospheric response to SST anomalies. part I: Background-state dependence, teleconnections, and local effects in winter. *Journal of the Atmospheric Sciences*, **75 (12)**, 4107 – 4124, https://doi.org/10.1175/JAS-D-17-0297.1, URL https://journals.ametsoc.org/view/journals/atsc/75/12/jas-d-17-0297.1.xml.

Accepted for publication in *Journal of Climate*. DOI 10.1175/JCLI-D-23-0015.1.

Titchner, H. A., and N. A. Rayner, 2014: The Met Office Hadley Centre sea ice and sea surface temperature data set, version 2: 1. sea ice concentrations. *Journal of Geophysical Research: Atmospheres*, **119 (6)**, 2864–2889, https://doi.org/https://doi.org/10.1002/2013JD020316.

Tseng, K.-C., E. Maloney, and E. Barnes, 2019: The consistency of MJO teleconnection patterns: An explanation using linear Rossby wave theory. *Journal of Climate*, **32 (2)**, 531 – 548, https://doi.org/10.1175/JCLI-D-18-0211.1.

Wallace, J. M., and D. S. Gutzler, 1981: Teleconnections in the geopotential height field during the Northern Hemisphere winter. *Monthly Weather Review*, **109 (4)**, 784 – 812, https://doi.org/10.1175/1520-0493(1981)109⟨0784:TITGHF⟩2.0.CO;2.

Wang, B., R. Wu, and X. Fu, 2000: Pacific–East Asian teleconnection: How does ENSO affect east Asian climate? *Journal of Climate*, **13 (9)**, 1517 – 1536, https://doi.org/10.1175/1520-0442(2000)013⟨1517:PEATHD⟩2.0.CO;2.

Wang, Z., T. Li, and Y. Sun, 2021: Interdecadal variability of intensity of the Madden–Julian oscillation. *Atmospheric Science Letters*, **22 (5)**, e1027, https://doi.org/https://doi.org/10.1002/asl.1027.

Webster, P. J., 1981: Mechanisms determining the atmospheric response to sea surface temperature anomalies. *Journal of Atmospheric Sciences*, **38 (3)**, 554 – 571, https://doi.org/https://doi.org/10.1175/1520-0469(1981)038⟨0554:MDTART⟩2.0.CO;2, URL https://journals.ametsoc.org/view/journals/atsc/38/3/1520-0469_1981_038_0554_mdtart_2_0_co_2.xml.

Wheeler, M. C., and H. H. Hendon, 2004: An all-season real-time multivariate MJO index: Development of an index for monitoring and prediction. *Monthly weather review*, **132 (8)**, 1917–1932, https://doi.org/10.1175/1520-0493(2004)132⟨1917:AARMMI⟩2.0.CO;2.

Wheeler, M. C., H. H. Hendon, S. Cleland, H. Meinke, and A. Donald, 2009: Impacts of the Madden–Julian Oscillation on Australian rainfall and circulation. *Journal of Climate*, **22 (6)**, 1482 – 1498, https://doi.org/10.1175/2008JCLI2595.1.

Wulff, C. O., R. J. Greatbatch, D. I. V. Domeisen, G. Gollan, and F. Hansen, 2017: Tropical forcing of the summer east Atlantic pattern. *Geophysical Research Letters*, **44 (21)**,

Accepted for publication in *Journal of Climate*. DOI 10.1175/JCLI-D-23-0015.1.

11,166–11,173, https://doi.org/https://doi.org/10.1002/2017GL075493, URL https://agupubs.onlinelibrary.wiley.com/doi/abs/10.1002/2017GL075493.

Zhang, C., 2005: Madden-Julian Oscillation. *Reviews of Geophysics*, **43 (2)**, https://doi.org/10.1029/2004RG000158.

Zhang, C., 2013: Madden–julian oscillation: Bridging weather and climate. *Bulletin of the American Meteorological Society*, **94 (12)**, 1849 – 1870, https://doi.org/https://doi.org/10.1175/BAMS-D-12-00026.1, URL https://journals.ametsoc.org/view/journals/bams/94/12/bams-d-12-00026.1.xml.

Zhou, S., M. L'Heureux, S. Weaver, and A. Kumar, 2012: A composite study of the MJO influence on the surface air temperature and precipitation over the continental United States. *Climate dynamics*, **38 (7)**, 1459–1471.

Zuckerberg, B., C. Strong, J. M. LaMontagne, S. S. George, J. L. Betancourt, and W. D. Koenig, 2020: Climate dipoles as continental drivers of plant and animal populations. *Trends in ecology & evolution*, **35 (5)**, 440–453, https://doi.org/10.1016/j.tree.2020.01.010.

Accepted for publication in *Journal of Climate*. DOI 10.1175/JCLI-D-23-0015.1.